CEREBRAL MICROBLEED DETECTION VIA FOURIER DESCRIPTOR WITH DUAL DOMAIN DISTRIBUTION MODELING

Hangfan Liu[1], Tanweer Rashid[1,2], Mohamad Habes[1,2]

1 Center for Biomedical Computing and Analysis, University of Pennsylvania, USA
2 Neuroimage Analytics Laboratory (NAL) and the Biggs Institute Neuroimaging Core (BINC), Glenn Biggs Institute for Neurodegenerative Disorders, University of Texas Health San Antonio (UTHSA), San Antonio, USA

ABSTRACT

In this study we propose a novel cerebral microbleed (CMB) detection technique which simultaneously utilizes distribution information in dual domains and shape information obtained by a Fourier descriptor, and does not rely on a large set of training data. Specifically, the dual domain distribution modeling aims to simultaneously examine the image content in both gradient domain and voxel domain, while the Fourier descriptor further characterize the shape of the candidate region. A set of labeled data is used to form the dual-domain distribution as well as the distribution of Fourier coefficients. Then the probability of a region containing a CMB is estimated by combining the two types of distributions. Experimental results show that the proposed approach is efficient and desirable for scenarios where the number of samples is limited.

Index Terms— Dual Domain Distribution, Fourier Descriptor, Cerebral Microbleed Detection.

1. INTRODUCTION

Cerebral microbleeds (CMB) are small hemosiderin-containing hemorrhages that are considered to be a type of small vessel ischemic disease [1]. In T2* gradient-recalled echo (GRE) or susceptibility weighted imaging (SWI) magnetic resonance images (MRI), CMBs typically appear as small rounded or ellipsoidal hypointense regions with a diameter of 2 to 10 millimeters [2, 3].CMBs have also been associated with increased risk of dementia, intracerebral hemorrhage, infarction and dementia [4]. Due to their small size, sporadic prevalence in the brain and presence of mimics such as enlarged perivascular spaces, infarcts and iron/calcium depositions, the detection/segmentation of CMBs can be difficult and time consuming for human raters. Studies have shown that SWI, being more sensitive to iron complexes, is more sensitive than T2* GRE for detecting CMBs [5-8].The appearance of CMBs on MR is dependent mostly on echo time and magnetic field strength [3, 6]. According to a study by Gregoire larger echo times in T2* GRE images at 1.5T field strength can result in poor image quality and increase the likelihood of cerebral microbleed mimics being observed [9], while other studies have shown that shorter echo times can be used at higher field strengths [6, 10].

Due to the consistent appearance, size and shape of CMBs, a number of studies have attempted to exploit these physical features for automated or semi-automated detection. Radial symmetry transform, a technique that enhances features with spherical geometry, has been used in [11, 12]. Ghafaryasl et al. used a sequence of two classifiers where the first classifier used geometric and intensity-based features and the second classifier used local image descriptors [13]. Seghier et al. [14] utilized a probabilistic tissue class model based on the segmentation framework of [15], with CMBs being treated as a separate atypical class to segment CMBs. Classical machine learning techniques have also been utilized. Fazlollahi et al. [16] used Random Forest (RF) classifiers where a multi-scale Laplacian of Gaussian is first used to select candidates, followed by generation of Radon-transform-based features which were used to a train multi-layer classification cascade composed of several RF classifiers. Barnes et al. used a Gaussian distribution-based local statistical thresholding to determine hypointense candidates, and then applied a Support Vector Machine (SVM) [17] to classify CMBs from other mimics. Chen et al. [18] proposed an automated method for detecting CMBs. Initially, a RF classifier to generate an initial set of CMB candidates based on intensity information, which is followed by hierarchical feature extraction using independent subspace analysis network and subsequent classification using SVM.

In this work we present a distribution-based method for detecting CMBs, which combines information contained in the distribution of

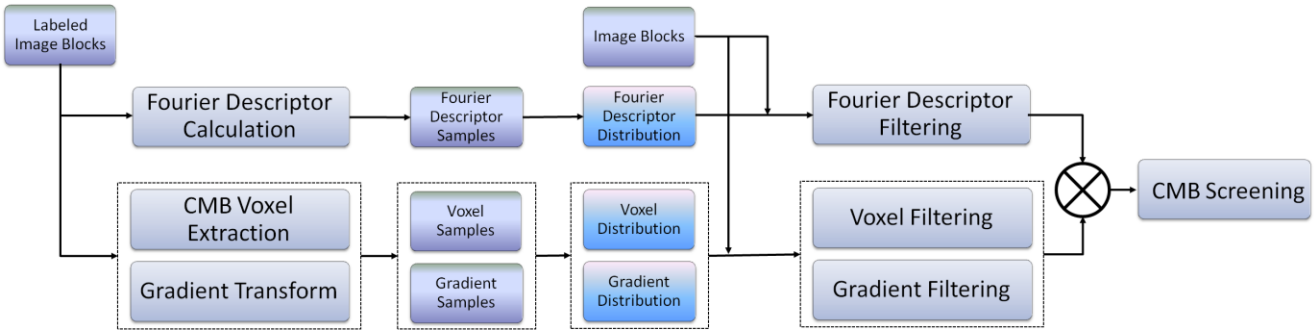

Fig. 1. Overall framework of the proposed approach.

978-1-7281-7401-3/20/$31.00 ©2020 IEEE

Fourier descriptors with that of voxels and gradients into a single resilient system. To our knowledge, no one has previously used Fourier descriptors for CMB segmentation. Specifically, we inspect the shape information contained in the images and exploit statistics of latent CMB components in both voxel domain and gradient domain. Such an approach does not rely on a large set of training data, which is desirable for scenarios where labeled data are insufficient.

2. METHOD

The proposed approach integrates Fourier descriptor distribution and dual domain distribution into a probabilistic system for cerebral microbleed (CMB) detection. Specifically, the probability of a voxel u contained within a CMB region is estimated as:

$$p(u) = g_{\mathcal{F}}(u) \cdot g_D(u), \tag{1}$$

where $g_{\mathcal{F}}(u)$ and $g_D(u)$ exploits Fourier descriptor distribution and dual-domain distribution, respectively. The overall framework of the proposed approach is illustrated in Fig. 1.

2.1. Fourier Descriptor Distribution

The Fourier descriptor [19] captures the shape information. In Eq. (1), $g_{\mathcal{F}}(u)$ is formulated as

$$g_{\mathcal{F}}(u) = \exp\left\{-\frac{\left\|E\circ\boldsymbol{\mathcal{F}}(\boldsymbol{u})-\bar{\boldsymbol{f}}\right\|_2^2}{\lambda_0}\right\}, \tag{2}$$

where $\boldsymbol{\mathcal{F}}(\boldsymbol{u})$ calculates the Fourier descriptors of the $S \times S$ block $\boldsymbol{u}$ centered at voxel u, E is the operator extracting the first N descriptors, $\bar{\boldsymbol{f}}$ is the expectation of such descriptors estimated from the training dataset, λ_0 is a parameter reflecting the reliability of the estimated $\bar{\boldsymbol{f}}$, which is proportional to the corresponding variance.

Specifically, in order to obtain the Fourier descriptors, we need to binarize the image first. Since the process of binarization is quite sensitive to noise, we adopted image denoising techniques [20-23] to reduce the influence of noise. We then remove the background and binarize image using Otsu's threshold τ, which divides the image voxels into 2 classes and minimizes the intra-class variance [24]:

$$\sigma^2(\tau) = w_1\sigma_1^2(\tau) + w_2\sigma_2^2(\tau), \tag{3}$$

where w_1 and w_2 are the weights decided by the probabilities of the 2 classes separated by τ, while σ_1^2 and σ_2^2 are the variances.

After binarization, we inspect the connected components found in the binary image and examine the shape and size of each candidate object. Specifically, we discard objects with more than M voxels, and then calculate the generic Fourier descriptors for the remaining objects. Such descriptors transform the images in polar space into a normal 2-dimensional rectangular image in Cartesian space so that the obtained features are rotation-invariant and compact [19].

Suppose there are n_t CMBs in the training data. In the learning stage, we retrieve the $S \times S$ blocks centered at the CMBs from the training data and calculate the Fourier descriptors $\boldsymbol{f}_i, i = 1, 2, \ldots, n_t$, then estimate $\bar{\boldsymbol{f}}$ as

$$\bar{\boldsymbol{f}} \doteq \frac{1}{n_t}\sum_1^{n_t}\boldsymbol{f}_i. \tag{4}$$

Based on the estimated expectations, it is not difficult to calculate the variances and thus determine the parameter λ_0.

2.2. Dual Domain Distribution

The dual domain distribution exploits statistics of CMB components in both voxel domain and gradient domain. In addition to the commonly used voxel/pixel domain method we integrate gradient information into the proposed system [25] because image gradients contain important visual information [26, 27] and play an important role in various applications [28, 29],. The term $g_D(u)$ in Eq. (1) is formulated as

$$g_D(u) = \exp\left\{-\frac{\|u-\bar{u}\|_2^2}{\lambda_1}\right\} \cdot \exp\left\{-\frac{\|\boldsymbol{g}-\bar{\boldsymbol{g}}\|_2^2}{\lambda_2}\right\}, \tag{5}$$

where λ_1 and λ_2 are the parameters determined by the variances of the distributions, $\bar{u}$ and $\bar{\boldsymbol{g}}$ are expectations of CMB components estimated in voxel domain and gradient domain respectively.

The gradients are obtained by applying first-order horizontal and vertical differential operators to the image [28, 29]. Besides such differences between adjacent voxels, in this work we take the sum of gradients within a space distance range of $R = r + \delta$ voxels into account to form the vector $\boldsymbol{g}$, where r is the maximum radius of CMBs, and δ is a small integer. The expectations $\bar{u}$ and $\bar{\boldsymbol{g}}$ as well as parameters λ_1 and λ_2 can be estimated in the same way as $\bar{\boldsymbol{f}}$ and λ_0 described in Section 2.1.

2.3. Final Estimation

After the probability $p(u)$ is computed over the whole image, the voxels in potential CMB regions can be included in a set $\mathbb{S}$:

$$\mathbb{S} = \{u \mid p(u) > \mathcal{T}\}, \tag{6}$$

where $\mathcal{T}$ is an empirically chosen threshold. In this paper we set $\mathcal{T} = 0.5$.

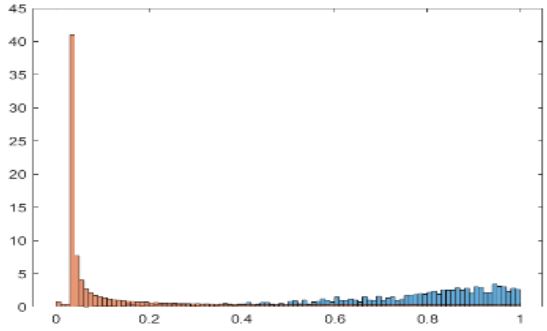

Fig. 2. Normalized distribution of $p(u)$ calculated on non-CMB voxels (red) and that calculated on CMB voxels (blue).

3. EXPERIMENTS

3.1. Data

We used 20 subject's 3T SWI data with expert segmentation made available from [30]. The images were acquired from a Philips scanner with repetition time of 17 ms and echo time of 24 ms. The images have a volume of 512x512x150, in-plane resolution of 0.45x0.45mm, slice thickness of 2mm and spacing of 1mm. The dataset was downloaded from http://www.cse.cuhk.edu.hk/~qdou/cmb-3dcnn/cmb-3dcnn.html.

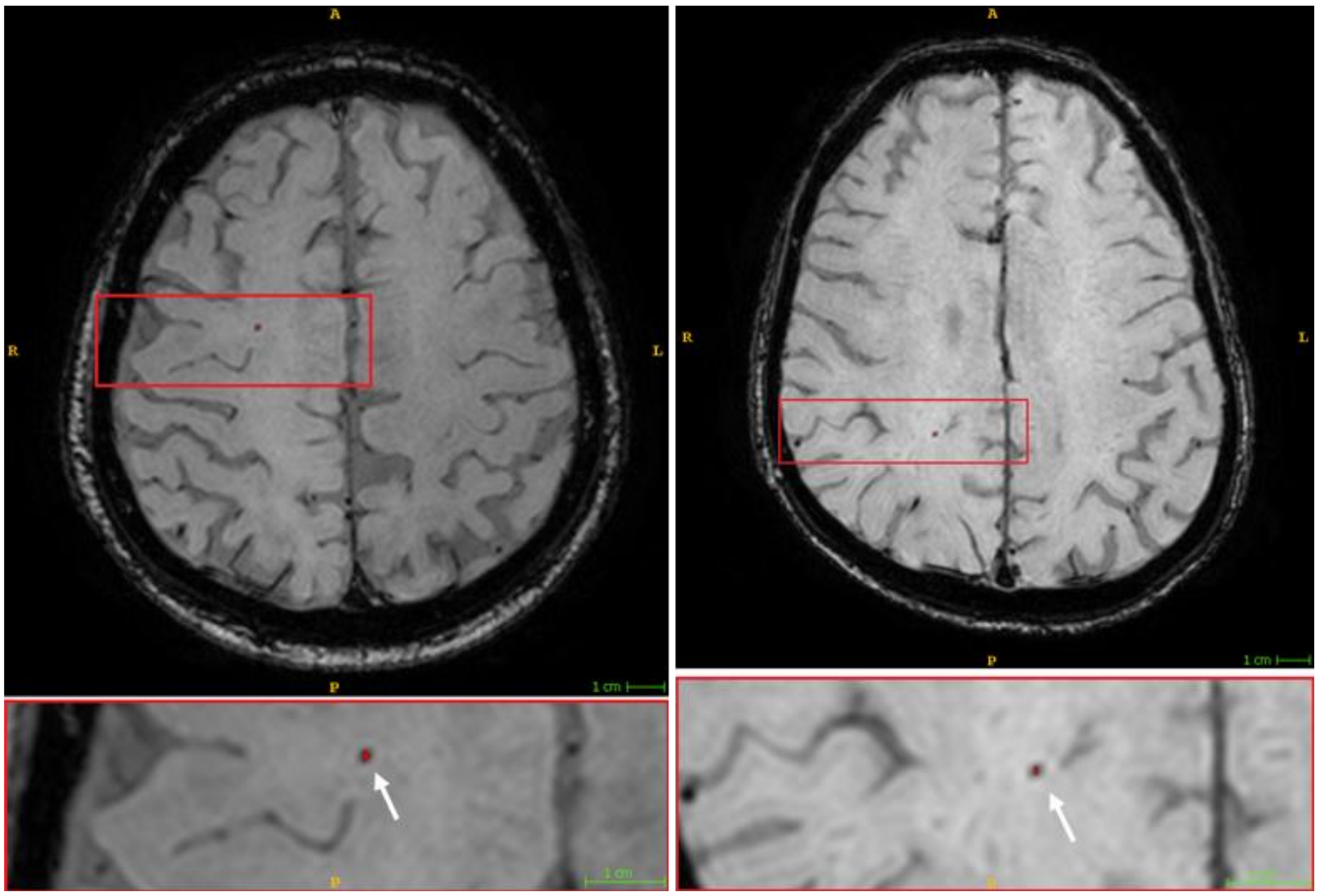

Fig. 3. Visualization of segmentation labels produced by the proposed approach applied to four different brain images. The detected CMB voxels are marked in red (white arrow in the zoomed insets).

3.1. Ability to Separate CMB

To test the ability of the proposed method to distinguish CMBs from other parts of the brain, we show the distribution of scores of non-CMB voxels and those of CMB voxels calculated by Eq. (1) in Fig. 2. Evidently, the scores of non-CMB voxels are concentrated near 0, while those of CMB voxels are generally above 0.5, thus the CMB components are well separated from the other parts of the image.

3.1. Detection Results

We evaluated the detection performance of the proposed method using the sensitivity S and precision P, which are calculated as

$$S = \frac{TP}{TP+FN}, \; P = \frac{TP}{TP+FP}, \tag{7}$$

where TP is the number of true positives, FN is that of false negatives, and FP stands for false positives. We first used the 10 subjects' data for distribution learning and parameter training, then used the remaining 10 subjects' data for testing. The proposed approach achieved a sensitivity of 85.2% and a precision of 3.2%. The relatively low precision is due to existence of scattered voxels that the model incorrectly classified as positive. The average number of false positive locations per subject is 69.5. Similar to previous semi-automated detection methods with high sensitivity but relatively low precision [11, 31], the false positive locations could be removed by a human rater or other screening techniques. Fig. 3 shows two examples of correctly classified CMBs in SWI. The detected voxels are marked in red.

4. CONCLUSIONS AND DISCUSSIONS

This paper presented a distribution modeling based approach to integrate the information contained in shapes as well as in both voxel and gradient domain. The shapes are characterized by Fourier descriptors after binarization with Otsu's threshold. Only a small set of labeled data is required to form the distributions. Experimental results show that the proposed approach could achieve relatively competitive sensitivity. The method could be used for preliminary screening, and can be desirable when the number of labeled data is limited. Since the proposed approach processes the images slice-wise, the multi-directional information in the 3 dimensional (3D) data is not fully utilized yet. How to better utilize the underlying correlation in the 3D image contents and combine with other effective techniques to build an improved system remains a future work.

ACKNOWLEDGEMENTS

This study was supported by National Institutes of Health grant R01 HL127659-04S1.

REFERENCES

[1] A. A. Gouw, A. Seewann, W. M. Van Der Flier,, *et al.*, "Heterogeneity of small vessel disease: a systematic review of MRI and histopathology correlations," *Journal of Neurology, Neurosurgery & Psychiatry,* vol. 82, pp. 126-135, 2011.

[2] S. M. Greenberg, M. W. Vernooij, C. Cordonnier, *et al.*, "Cerebral microbleeds: a guide to detection and interpretation," *The Lancet Neurology,* vol. 8, pp. 165-174, 2009.

[3] S. Haller, M. W. Vernooij, J. P. Kuijer, *et al.*, "Cerebral microbleeds: imaging and clinical significance," *Radiology,* vol. 287, pp. 11-28, 2018.

[4] S. Akoudad, F. J. Wolters, A. Viswanathan, R. F. de Bruijn, A. van der Lugt, A. Hofman, *et al.*, "Association of cerebral microbleeds with cognitive decline and dementia," *JAMA neurology,* vol. 73, pp. 934-943, 2016.

[5] Y. Shi and J. M. Wardlaw, "Update on cerebral small vessel disease: a dynamic whole-brain disease," *Stroke and Vascular Neurology,* vol. 1, pp. 83-92, 2016.

[6] R. Nandigam, A. Viswanathan, P. Delgado, M. Skehan, E. Smith, J. Rosand, *et al.*, "MR imaging detection of cerebral microbleeds: effect of susceptibility-weighted imaging, section thickness, and field strength," *American Journal of Neuroradiology,* vol. 30, pp. 338-343, 2009.

[7] M. Conijn, M. Geerlings, G.-J. Biessels, T. Takahara, T. Witkamp, J. Zwanenburg, *et al.*, "Cerebral microbleeds on MR imaging: comparison between 1.5 and 7T," *American journal of neuroradiology,* vol. 32, pp. 1043-1049, 2011.

[8] M. Ayaz, A. S. Boikov, E. M. Haacke, D. K. Kido, and W. M. Kirsch, "Imaging cerebral microbleeds using susceptibility weighted imaging: one step toward detecting vascular dementia," *Journal of Magnetic Resonance Imaging,* vol. 31, pp. 142-148, 2010.

[9] S. Gregoire, D. Werring, U. Chaudhary, J. Thornton, M. Brown, *et al.*, "Choice of echo time on GRE T2*-weighted MRI influences the classification of brain microbleeds," *Clinical radiology,* vol. 65, pp. 391-394, 2010.

[10] C. Stehling, H. Wersching, S. P. Kloska, P. Kirchhof, J. Ring, I. Nassenstein, *et al.*, "Detection of asymptomatic cerebral microbleeds: a comparative study at 1.5 and 3.0 T," *Academic radiology,* vol. 15, pp. 895-900, 2008.

[11] H. J. Kuijf, J. de Bresser, M. I. Geerlings, *et al.*, "Efficient detection of cerebral microbleeds on 7.0 T MR images using the radial symmetry transform," *NeuroImage,* vol. 59, pp. 2266-2273, 2012.

[12] W. Bian, C. P. Hess, S. M. Chang, S. J. Nelson, and J. M. Lupo, "Computer-aided detection of radiation-induced cerebral microbleeds on susceptibility-weighted MR images," *NeuroImage: Clinical,* vol. 2, pp. 282-290, 2013.

[13] B. Ghafaryasl, F. van der Lijn, M. Poels, W. J. Niessen, *et al.*, "A computer aided detection system for cerebral microbleeds in brain MRI," in *IEEE International Symposium on Biomedical Imaging*, 2012, pp. 138-141.

[14] M. L. Seghier, M. A. Kolanko, A. P. Leff, H. R. Jäger, S. M. Gregoire, and D. J. Werring, "Microbleed detection using automated segmentation (MIDAS): a new method applicable to standard clinical MR images," *PloS One,* vol. 6, p. e17547, 2011.

[15] J. Ashburner and K. J. Friston, "Unified segmentation," *Neuroimage,* vol. 26, pp. 839-851, 2005.

[16] A. Fazlollahi, F. Meriaudeau, V. L. Villemagne, *et al.*, "Efficient machine learning framework for computer-aided detection of cerebral microbleeds using the radon transform," in *IEEE International Symposium on Biomedical Imaging*, 2014, pp. 113-116.

[17] S. R. Barnes, E. M. Haacke, M. Ayaz, A. S. Boikov, W. Kirsch, and D. Kido, "Semiautomated detection of cerebral microbleeds in magnetic resonance images," *Magnetic Resonance Imaging,* vol. 29, pp. 844-852, 2011.

[18] Q. Dou, H. Chen, L. Yu, *et al.*, "Automatic cerebral microbleeds detection from MR images via independent subspace analysis based hierarchical features," in *International Conference of the IEEE Engineering in Medicine and Biology Society*, 2015, pp. 7933-7936.

[19] D. Zhang and G. Lu, "Shape-based image retrieval using generic Fourier descriptor," *Signal Processing: Image Communication,* vol. 17, pp. 825-848, 2002.

[20] H. Liu, X. Zhang, and R. Xiong, "Content-adaptive low rank regularization for image denoising," in *IEEE International Conference on Image Processing*, 2016, pp. 3091-3095.

[21] H. Liu, R. Xiong, J. Zhang, and W. Gao, "Image denoising via adaptive soft-thresholding based on non-local samples," in *IEEE Conference on Computer Vision and Pattern Recognition*, 2015, pp. 484-492.

[22] Y. Zhang, R. Kang, X. Peng, *et al.*, "Image denoising via structure-constrained low-rank approximation," *Neural Computing and Applications,* 2020.

[23] H. Liu, R. Xiong, D. Liu, F. Wu, and W. Gao, "Low rank regularization exploiting intra and inter patch correlation for image denoising," in *IEEE Visual Communications and Image Processing*, 2017.

[24] N. Otsu, "A threshold selection method from gray-level histograms," *IEEE Transactions on Systems, Man, and Cybernetics,* vol. 9, pp. 62-66, 1979.

[25] A. Buades, B. Coll, and J.-M. Morel, "A non-local algorithm for image denoising," in *IEEE Conference on Computer Vision and Pattern Recognition,* 2005, pp. 60-65.

[26] H. Liu, R. Xiong, X. Fan, *et al.*, "Compressive gradient based scalable image SoftCast," in *IEEE Visual Communications and Image Processing*, 2017.

[27] J. Zhu and N. Wang, "Image quality assessment by visual gradient similarity," *IEEE Transactions on Image Processing,* vol. 21, pp. 919-933, 2011.

[28] H. Liu, R. Xiong, X. Zhang, Y. Zhang, S. Ma, and W. Gao, "Nonlocal gradient sparsity regularization for image restoration," *IEEE Transactions on Circuits and Systems for Video Technology,* vol. 27, pp. 1909-1921, 2017.

[29] H. Liu, R. Xiong, Q. Song, F. Wu, and W. Gao, "Image super-resolution based on adaptive joint distribution modeling," in *IEEE Visual Communications and Image Processing*, 2017.

[30] Q. Dou, H. Chen, L. Yu, *et al.*, "Automatic detection of cerebral microbleeds from MR images via 3D convolutional neural networks," *IEEE Transactions on Medical Imaging,* vol. 35, pp. 1182-1195, 2016.

[31] H. J. Kuijf, M. Brundel, J. de Bresser, *et al.*, "Semi-automated detection of cerebral microbleeds on 3.0 T MR images," *PLoS One,* vol. 8, 2013.